Journal of Solid State Electrochemistry (2019) 23:3123–3133
https://doi.org/10.1007/s10008-019-04410-6

ORIGINAL PAPER

Development of a Randles-Ševčík-like equation to predict the peak current of cyclic voltammetry for solid metal hexacyanoferrates

O. A. González-Meza[1] · E. R. Larios-Durán[1] · A. Gutiérrez-Becerra[2] · N. Casillas[3] · J. I. Escalante[3] · M. Bárcena-Soto[3]

Received: 24 January 2019 / Revised: 12 September 2019 / Accepted: 17 September 2019 / Published online: 22 October 2019

Abstract

A mathematical model, derived from Fick's second law for planar and spherical coordinates, is presented and solved to obtain novel equations that satisfactorily predict the charge transfer and peak current observed in cyclic voltammetry of solid hexacyanoferrates. For a planar geometry, two cases are considered. The first one takes into account the effect of the evolution of the activities of the oxidized and reduced phases of the hexacyanoferrates on the peak currents, while in the second one, the activities of both phases were considered as a constant. In the first case, an analysis of charges involved in the reaction is required to obtain the molar fractions of the oxidized and reduced forms of the hexacyanoferrates. In this case, the solution of the model is obtained numerically using the lines method. In the second case, the model is analytically solved obtaining a Randles-Ševčík-like equation. When spherical coordinates are considered, the activities of the solid phase are assumed to be constant and the model is analytically solved. In this way, other novel equations allowing the calculus of the electroactive electrode area and the diffusion coefficient of the alkali ions are presented. The advantages of an analytical expression for the peak current as a function of the square root of the potential scan rate, instead of a numerical solution, are analyzed. The validity of each model is proven by its comparison with experimental measurements for peak currents in a carbon paste electrode containing nickel hexacyanoferrate immersed in a 0.5M KNO_3 solution.

Keywords Nickel hexacyanoferrate · Randles-Ševčík · Diffusion coefficient · Peak current

Introduction

Transition metal hexacyanoferrates (M′HCF), written in their oxidized or reduced state as MM′$[Fe^{(III)}(CN)_6]$ and M_2M′$[Fe^{(II)}(CN)_6]$ respectively, are materials that possess interesting electrochromic and electrochemical properties as well as magnetic, zeolitic, and reversible redox behavior [1–3]. These characteristics make them valuable materials in several technology areas such as the production of electrochromic screens [4, 5], catalysis [6], photosensitive devices [7], ion-selective sensors [8], and energy storage devices [9–11]. Due to their nature, M′HCF are natural candidates to be characterized by electrochemical techniques through the use of modified electrodes elaborated by fixing some crystals of M′HCF either in a paste [12] or on composite electrodes of graphite, paraffin, and M′HCF [13]. However, in both cases, the crystals are randomly distributed in the carbon matrix, making determining the real electroactive area of the electrode difficult, avoiding a complete physical characterization of this material, e.g., the calculation of the diffusion coefficient of the alkali ions inserting in the M′HCF lattice. Some studies [13–16] try to overcome this inconvenience using linear or cyclic voltammetry and applying the Randles-Ševčík equation to calculate such parameters. However, it should be highlighted that the Randles-Ševčík equation, which predicts I_p in linear or cyclic voltammetry for reversible and diffusion-controlled electron transfer processes [17], was derived assuming the following simple reversible reaction [18, 19]:

$$O + ne^- \rightleftarrows R \quad (1)$$

where the specie O, initially present in bulk solution, diffuses and subsequently is reduced on the electrode surface to form

✉ M. Bárcena-Soto
maxbar@gmx.net

[1] Departamento de Ingeniería Química, CUCEI, Universidad de Guadalajara, Guadalajara, Mexico

[2] Departamento de Ciencias Básicas y Aplicadas, CUTonalá, Universidad de Guadalajara, Guadalajara, Mexico

[3] Departamento de Química, CUCEI, Universidad de Guadalajara, Guadalajara, Mexico

the specie R by accepting n electrons. Once R is formed, it diffuses into the bulk of the solution. Fick's second law for this process is solved with two boundary conditions for each species: the first boundary condition describes that at certain distance from the electrode, $x \to \infty$, the concentration of R, or O, is constant and corresponds to that in the bulk of the solution. The second boundary condition expresses that the concentration of R, or O, varies depending on the applied polarization potential, according with the Nernst equation. Thus, it is possible to derive a mathematical model that describes the voltammetric behavior of the reaction (1).

In 1948, Randles [18] and Ševčík [19] independently solved the model in Cartesian coordinates; later in 1964, Nicholson and Shain [20] revisited the solution and solved it, not only in Cartesian but also in spherical coordinates. In both cases, an analytical solution could not be obtained, so a numerical approach was necessary. After a numerical analysis, I_p was found as a function of n, v, D_O, T, A, and C_O^* for rectangular coordinates; as is observed in the Randles-Ševčík equation,

$$I_p = 0.4463nFAC_O^*\left(D_O\frac{nF}{RT}v\right)^{1/2} \quad (2)$$

A plot of I_p vs. $v^{1/2}$ gives a straight line with the slope $0.4463nFAC_O^*\left(D_O\frac{nF}{RT}\right)^{1/2}$ and zero intercept.

It should be highlighted that the electrochemical process involved in (1), where the diffusion of O and R takes place in liquid phase, is different to the one involved in M′HCF modified electrodes, where the diffusion and insertion of alkali ions into the M′HCF lattice and the simultaneous oxidation and reduction occur in the solid phase. The general electrochemical reaction of a solid M′HCF can be written as follows [21]:

$$MM'\left[Fe^{(III)}(CN)_6\right]_{(s)} + M^+ + e^- \rightleftarrows M_2M'\left[Fe^{(II)}(CN)_6\right]_{(s)} \quad (3)$$

where M^+ is an alkali cation in solution diffusing and inserting into the M′HCF lattice and M′ is the nitrogen coordinated metal ion. In order to simplify the nomenclature, ω and ρ will be used hereafter instead of $MM'[Fe^{(III)}(CN)_6]_{(s)}$ and $M_2M'[Fe^{(II)}(CN)_6]_{(s)}$respectively throughout the text.

Despite the significant differences between the reactions (1) and (3), the Randles-Ševčík equation and its linear dependence of I_p on $v^{1/2}$ are frequently used to estimate both the diffusion coefficients of alkali ions in the M′HCF lattices and the electroactive area of M′HCF modified electrodes. An example is the paper of Kahlert et al. [13], where the Randles-Ševčík equation is employed to estimate the diffusion coefficient of K^+ ions in copper hexacyanoferrate (CuHCF) fixed on a composite graphite electrode. There, the concentration of active centers of solid CuHCF instead of the bulk concentration of K^+ ions in solution was considered, accepting that the Randles-Ševčík equation is valid for solid-phase reactions. This approach provides diffusion coefficient values for K^+ at around 1×10^{-9} cm^2 s^{-1}. These values were corroborated with electrochemical impedance spectroscopy (EIS), which produced similar results. However, the EIS spectra were interpreted assuming that a Warburg element, which is derived for diffusional processes in solution [22], is able to describe also diffusional processes in the solid phases. In order to calculate the electroactive area of the electrode, the authors [13] have carried out chronoamperometric measurements, which indicated that this area is approximately 80 times smaller than the geometric electrode area. The difference between geometrical and real area has been ascribed to the fact that not all the CuHCF particles are active, as some of them either lack the contact to graphite or to the electrolyte solution. Once the area was known, the Randles-Ševčík equation has been used to calculate the diffusion coefficient.

On the other hand, Heli et al. [14] describe the sensing of N-acetyl-L cysteine using a transducer of cobalt hexacyanoferrate (CoHCF) nanoparticles and computed the diffusion coefficient of Na^+ ions in CoHCF using Randles-Ševčík equation. Unlike Kahlert et al., Heli et al. considered that the adequate concentration is the Na^+ bulk concentration; however, even though the experimental I_p vs. $v^{1/2}$ lineal plot presents an intercept not predicted by the Randles-Ševčík equation, it was employed to calculate the diffusion coefficient, reporting values in the order of 2×10^{-5} cm^2 s^{-1}. No explanation about the intercept was given. Gholivand and Azadbakht [16] reported similar results. They obtained non-zero intercept in their experimental I_p vs. $v^{1/2}$ plots, and even so, the Randles-Ševčík equation was employed to calculate the diffusion coefficient of K^+ ion in zirconium hexacyanoferrate (ZrHCF).

Only some papers deal with the charge propagation in solid M′HCFs in a more rigorous manner; among which, the papers of Lovrić et al. [23] and Schröder et al. [24] should be mentioned. Lovrić et al. have developed a theoretical analysis for charge transfer reaction at the three-phase junction using a two-dimensional semi-infinite model, which considers the diffusion of electrons and ions within the crystal lattice. They conclude that the net current is the sum of both the surface and the bulk current; however, the former can be negligible in cases where the bulk reaction is dominating. On the other hand, Schröder et al. have presented a numerical simulation for a single crystal potential-step experiment in order to understand the electrochemical conversion of an immobilized particle on an electrode. They also evaluated the possibility to derive geometric parameters or individual diffusion coefficients from a chronoamperometric curve, concluding that the electrochemical reduction depends on the crystal geometry, which in some cases can be simulated using two- or three-dimensional models. As Schröder et al. claim in [24], it is mandatory to combine theoretical and experimental efforts to reach a better understanding of the mechanisms of the insertion in solid-state electrochemical reactions.

In this work, a model is presented to predict the peak current I_p associated with the charge transfer in solid M′HCFs. The model provides a Randles-Ševčík-like equation considering the chemical reaction (3) in which the oxidation and reduction of solid M′HCF in conjunction with the insertion of an alkali ion is considered, instead of reaction (1). The objective of this work is to contribute a fundamental understanding of the phenomenological aspects associated with the electrochemical reactions in solid M′HCF, providing an explanation of the well-known non-zero intercept in I_p vs. $v^{1/2}$ plots. As in the Randles-Ševčík procedure, here, Fick's second law was solved taking into account the proper boundary conditions. The resulting model can be solved both numerically and, under certain considerations, analytically. In order to validate the model, the peak currents I_p were used which were experimentally measured at several scan rates v, for a carbon paste electrode containing nickel hexacyanoferrate (NiHCF) immersed in a 0.5-M KNO_3 solution.

Theoretical framework

A fast electron transfer reaction (3) and equilibrium at the electrode surface allow to formulate the Nernst equation as follows:

$$E = E^{\circ} + \frac{RT}{nF}\ln\left(\frac{a_{\omega}a_{M^+}}{a_{\rho}}\right) \tag{4}$$

Since the activity a_i is related to the concentration C_i and the activity coefficient γ_i, Eq. (4) can be expressed as

$$E = E^{\circ} + \frac{RT}{nF}\ln\left(\frac{\gamma_{\omega}}{\gamma_{\rho}}\right) + \frac{RT}{nF}\ln(\gamma_{M^+}) + \frac{RT}{nF}ln\left(\frac{C_{\omega}}{C_{\rho}}\right) + \frac{RT}{nF}\ln[C_{M^+}(0,t)] \tag{5}$$

Furthermore, if the concentrations of solid species, ω (MM′$[Fe^{(III)}(CN)_6]_{(s)}$) and ρ ($M_2M'[Fe^{(II)}(CN)_6]_{(s)}$) for reaction (3), are written in terms of $X_{\omega}(t)$ as Lovrić et al., suggested [25], then Eq. (5) is given as

$$E = E^{\circ} + \frac{RT}{nF}\ln\left(\frac{\gamma_{\omega}}{\gamma_{\rho}}\right) + \frac{RT}{nF}\ln(\gamma_{M^+}) + \frac{RT}{nF}\ln\left(\frac{X_{\omega}(t)}{1-X_{\omega}(t)}\right) + \frac{RT}{nF}\ln[C_{M^+}(0,t)] \tag{6}$$

The first three terms in (6) can be regarded as the formal potential of reaction (3). Subsequently, the Nernst equation for reaction (3) is expressed as

$$E = E^{\circ'} + \frac{RT}{nF}\ln\left(\frac{X_{\omega}(t)}{1-X_{\omega}(t)}\right) + \frac{RT}{nF}\ln[C_{M^+}(0,t)] \tag{7}$$

Then the formal potential follows as

$$E^{\circ'} = E_{eq} - \frac{RT}{nF}\ln\left(\frac{X_{\omega}^{eq}}{1-X_{\omega}^{eq}}\right) - \frac{RT}{nF}\ln\left(C_{M^+}^{*}\right) \tag{8}$$

At this point, it is necessary to remember that for linear sweep voltammetry, E will decrease linearly as follows:

$$E = E_{eq} - vt \tag{9}$$

where E can be expressed by substituting (8) in the Nernst equation (7):

$$E = E_{eq} - \frac{RT}{nF}\ln\left(\frac{X_{\omega}^{eq}}{1-X_{\omega}^{eq}}\right) - \frac{RT}{nF}\ln\left(C_{M^+}^{*}\right) + \frac{RT}{nF}\ln\left(\frac{X_{\omega}(t)}{1-X_{\omega}(t)}\right) + \frac{RT}{nF}\ln(C_{M^+}(0,t)) \tag{10}$$

By substituting (9) in (10), the following expression is obtained:

$$E_{eq} - vt = E_{eq} + \frac{RT}{nF}\ln\left(\frac{1-X_{\omega}^{eq}}{X_{\omega}^{eq}}\frac{X_{\omega}(t)}{1-X_{\omega}(t)}\right) + \frac{RT}{nF}\ln\left(\frac{C_{M^+}(0,t)}{C_{M^+}^{*}}\right) \tag{11}$$

Equation (11) establishes, in a thermodynamic way, a relationship between the concentration of the alkali ion and the time elapsed in a voltammetric experiment.

Considering reaction (3), assuming unidirectional mass transport towards the M′HCF modified electrode and neglecting convective and migrational contributions, the transient M^+ concentration can be described by the Fick's second law:

$$\frac{\partial C_{M^+}(x,t)}{\partial t} = D_{M^+}\frac{\partial^2 C_{M^+}(x,t)}{\partial x^2} \qquad x \geq 0, \quad t \geq 0 \tag{12a}$$

with the following initial and boundary conditions:

$$C_{M^+}(x,0) = C_{M^+}^{*} \tag{12b}$$

$$\lim_{x\to\infty} C_{M^+}(x,t) = C_{M^+}^{*} \tag{12c}$$

$$C_{M^+}(0,t) = \frac{1-X_{\omega}(t)}{X_{\omega}(t)}\frac{X_{\omega}^{eq}}{1-X_{\omega}^{eq}}C_{M^+}^{*}\exp(-bt) \tag{12d}$$

A schematic diagram for the model described by Eq. (12a,b,c,d) is given in Fig. 1.

Initial condition (12b) describes an electrolyte solution initially containing M^+ at the bulk concentration $C_{M^+}^{*}$. (12c) relates to a constant concentration of M^+ at semi-infinite distance from the M′HCF modified electrode. These two conditions are quite similar to those used for Randles-Ševčík [18, 19] and Nicholson and Shain [20]. The main difference between their

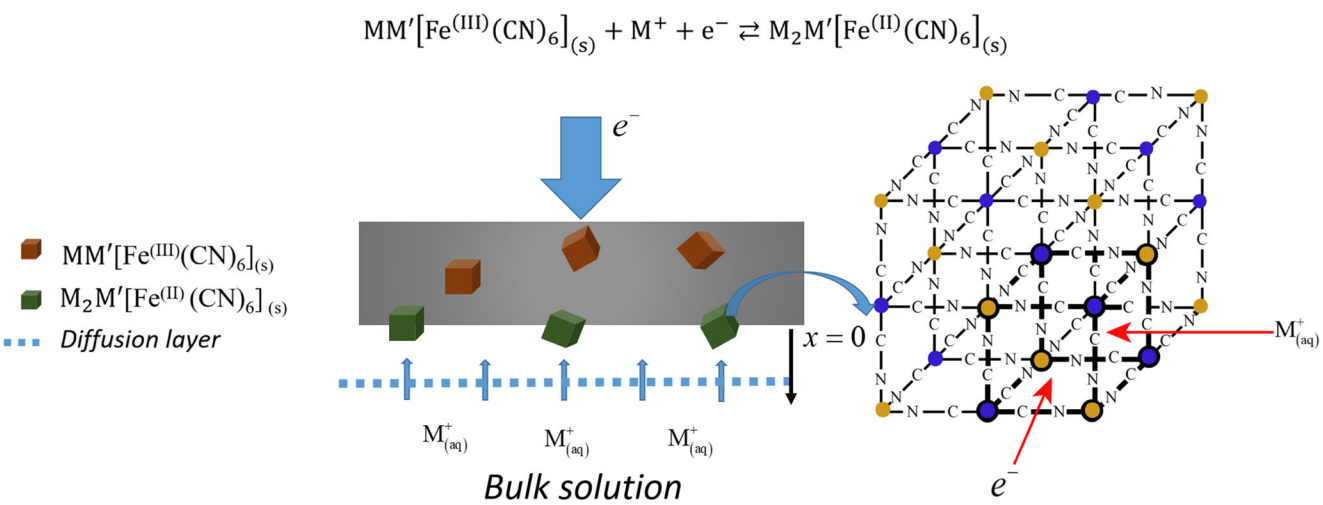

Fig. 1 Representation of a portion of crystalline matrix where both oxidized and reduced phases of hexacyanoferrate can be seen. ○ represents the nickel linked with nitrogen atoms and ● represents the iron linked with carbon atoms

approach and the one presented in this work is the condition (12d), which is deduced by solving Eq. (11) for $C_{M^+}(0,t)$.

Once the model described in (12) is numerically solved $C_{M^+}(x,t)$, its time derivative can be calculated and solved for $x=0$. Then, the current describing the flux of M^+ is obtained using Fick's first law [17]:

$$I(t) = -nFAD_{M^+}\left.\frac{\partial C_{M^+}(x,t)}{\partial t}\right|_{x=0} \tag{13}$$

It should be noticed that, in order to solve the model (12), it is necessary to know X_ω^{eq} as well as the evolution of the mole fraction of $X_\omega(t)$. Since $E^{\circ\prime}$ has been reported for several M′ HCF [26], and E_{eq} as well as $C^*_{M^+}$ can be determined experimentally, X_ω^{eq} can be readily obtained from Eq. (8). On the other hand, there are some methods to compute $X_\omega(t)$ [27]; one of them uses the numerical calculus of the transient charge related to reaction (3), which requires experimental measurements.

In this work, in order to validate the theoretical model (12), a particular electrochemical interface, namely NiHCF modified electrode/ KNO_3 electrolyte, was experimentally studied by cyclic voltammetry. The details of the experimental measurements, the calculus of the transient charge, and the obtaining $X_\omega(t)$ are presented here. The numerical solution of the model and the current response provided by Eq. (13) are described in the following sections.

Experimental

Preparation of NiHCF

NiHCF was prepared by mixing 10 mL of 0.01M $NiCl_2$ solution ($NiCl_2 \cdot 6H_2O$, 99% from Golden Bell) with 10 mL of 0.01M $K_3[Fe(CN)_6]$ solution (J. T. Baker). The dissolution was centrifuged at 3000 rpm for 10 min and washed with distilled water. The precipitates were dried at 40°C under vacuum for 12 h and subsequently milled in an agate mortar to obtain fine crystals of NiHCF.

Preparation of the NiHCF modified electrode

The modified electrode was prepared by using carbon paste, which incorporates fine crystalline NiHCF. The paste was made by mixing 0.475 g of graphite powder (Sigma Aldrich) and 0.025 g of previously synthetized NiHCF with 0.5 mL of Nujol oil (Sigma Aldrich) to obtain a homogeneous and pasty material with a resistance value not bigger than 10 Ω for the assembled electrode. This material was placed inside a syringe; its piston allowed compacting the material and renewal of the electrode surface area, which had a diameter around of 5 mm. The carbon paste was contacted by a copper wire.

Electrochemical measurements

A conventional three-electrode cell was employed. The carbon paste modified electrode with the NiHCF was used as working electrode (0.1963 cm^2 geometrical area). A platinum foil was used as counter electrode, while a saturated calomel electrode (SCE) was used as reference. KNO_3 0.5 M was used as electrolyte solution.

Cyclic voltammetry measurements were carried out at scan rates between 20 and 100 V s^{-1}, starting from the open circuit potential (0.335 V vs. SCE) in anodic direction, in a polarization range from − 0.4 to 1.1 V vs. SCE, at 25 °C and atmospheric pressure. In all cases, a potentiostat Autolab PGSTAT 128N was used. The data were collected using Nova 2.0 software. All peak currents shown in Table 1 are reported taking into account a

Table 1 Anodic and cathodic charges defined in (15) for different v

v mVs^{-1}	$(Q_a)_v$ (C) × 10^3	$(Q_c)_v$ (C) × 10^3	$(X_\omega)_a$	$(X_\omega)_c$
20	2.8	− 2.9	0.13	0.15
30	2.3	− 2.4	0.11	0.12
40	2	− 2.0	0.09	0.1
50	1.8	− 1.8	0.08	0.09
60	1.6	− 1.7	0.07	0.09
70	1.6	− 1.6	0.07	0.08
80	1.5	− 1.5	0.07	0.08
90	1.4	− 1.4	0.06	0.07
100	1.3	− 1.4	0.06	0.07

baseline correction with the purpose of not considering the contribution of the capacitive current. Base line correction was carried out using the methodology described in [17].

Results and discussion

The electrochemical response of the NiHCF modified electrode immersed in KNO_3 solution and numerical calculation of $X_\omega(t)$

Figure 2 shows the experimental cyclic voltammograms at different scan rates for the NiHCF modified electrode immerse in the electrolyte solution. Figure 2 clearly depicts the anodic and cathodic responses associated to the following equilibrium:

$$KNi\left[Fe^{(III)}(CN)_6\right]_{(s)} + K^+_{(aq)} + e^- \rightleftarrows K_2Ni\left[Fe^{(II)}(CN)_6\right]_{(s)} \quad (14)$$

which is a particular case of reaction (3).

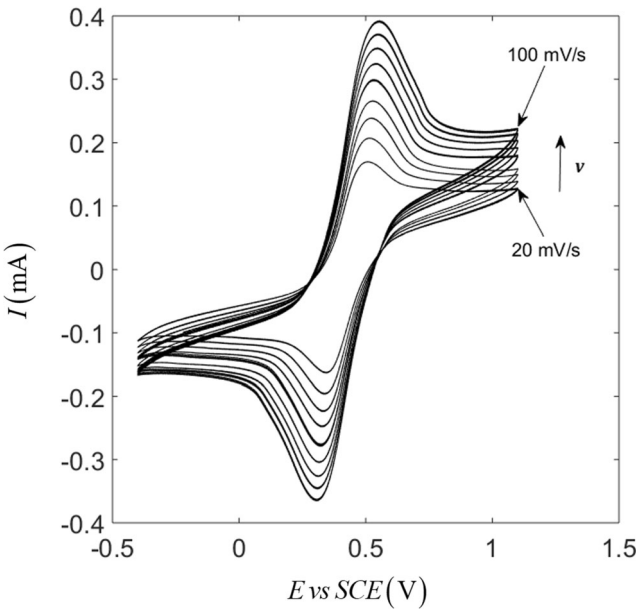

Fig. 2 Experimental cyclic voltammograms at different scan rates (20–100 mV s^{-1}) for NiHCF modified electrode in 0.5M KNO_3 solution

The voltammetric responses illustrated in Fig. 2 allow the numerical calculation of the charge transferred as a function of time, which is due to the formation of the mole fraction of $KNi[Fe^{(III)}(CN)_6]_{(s)}$ in reaction (14) from right to left side. Table 1 presents $(Q_a)_v$ and $(Q_c)_v$, for the polarization range depicted in each cyclic voltammogram shown in Fig. 2. The linear behavior of $1/|(Q_a)_v|$ and $1/|(Q_c)_v|$, generalized as $1/|(Q)_v|$, as a function of $v^{1/2}$ is shown in Fig. 3. The maximum possible charge for the anodic and cathodic process is determined by extrapolating $1/(Q_a)_v$ or $1/(Q_c)_v$ to $v = 0$ mV s^{-1}. This value corresponds to 0.021 C and 0.019 C for the anodic and cathodic charge respectively, and it is related to the maximum amount of mole of $KNi[Fe^{(III)}(CN)_6]_{(s)}$ or $K_2Ni[Fe^{(II)}(CN)_6]_{(s)}$ reacting in (14). Then, X_ω at $v > 0$, for the whole anodic or cathodic polarization range studied, can be defined as follows:

$$(X_\omega)_a = \frac{(Q_a)_v}{(Q_a)_{v=0}} \quad (15a)$$

$$(X_\omega)_c = \frac{(Q_c)_v}{(Q_c)_{v=0}} \quad (15b)$$

Table 1 summarizes these values for each scan rate.

The evolution of $X_\omega(t)$ can be computed from Fig. 2 according to

$$X_\omega(t) = \frac{Q_a(t)|_v}{(Q_a)_{v=0}} \quad (16)$$

Figure 4 shows, as an example, the graphical response of $Q_a(t)|_v$ at v=20 mV s^{-1} and its corresponding $X_\omega(t)$ value as a function of the polarization potential.

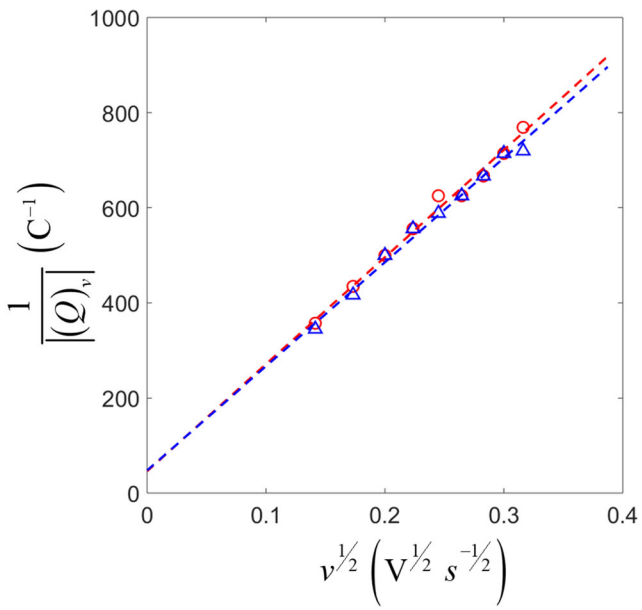

Fig. 3 Reciprocal total anodic (red) and cathodic (blue) charge vs. $v^{1/2}$

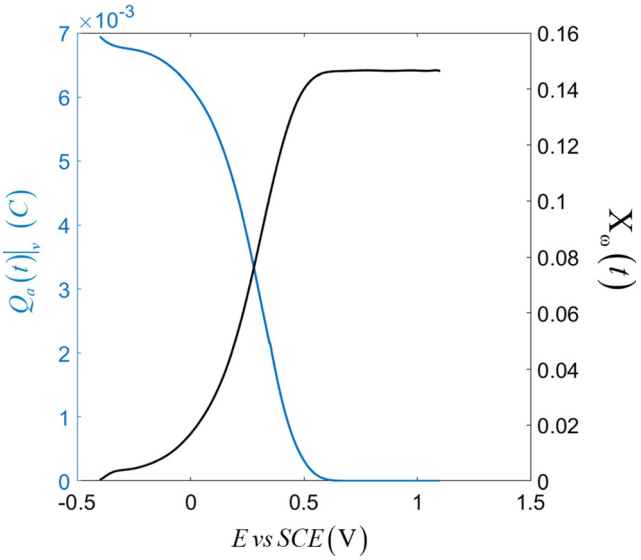

Fig. 4 Cathodic charge (blue) and molar fraction calculated from Eq. (16) (black) as a potential function for $v = 20$ mV s^{-1}

On the other hand, X_ω^{eq} can be calculated from Eq. (8) assuming a bulk concentration of KNO_3 of 0.5 M, an equilibrium potential experimentally measured of 0.335 V vs. SCE, and the formal potential of 0.522 V vs. SCE as it was reported in [26]. According to the calculation, the X_ω^{eq} value corresponds to 3.956×10^{-5}, indicating that at the equilibrium, the $K_2Ni[Fe^{(II)}(CN)_6]_{(s)}$ species is thermodynamically favored, as it was also found earlier [21].

Once X_ω^{eq} and $X_\omega(t)$ are determined, the model given in (12) can be numerically solved and subsequently, the current as a function of time can be computed.

Numerical solution of the proposed model and its comparison with the experimental measurements

The numerical solution of Eq. (12a,b,c,d) required its discretization to produce a system of ordinary differential equations which were solved by the second-order modified Rosenbrock method by using MatLab® software.

Figure 5a shows the theoretical cyclic voltammetry obtained numerically at several scan rates. The linear dependence of I_p vs. $v^{1/2}$could be predicted evaluating (13) at its maximum for anodic and cathodic branches. Its comparison with the experimental response of the NiHCF modified electrode/KNO_3 interface is shown in Fig. 5b. In all cases, X_ω^{eq} equals to 3.956×10^{-5}, a diffusion coefficient of K^+ of 1.29×10^{-5} cm^2 s^{-1} [28] and 0.335 V vs. SCE as equilibrium potential were fixed values, while the electroactive area was considered as a fitted parameter in the numerical solution. The optimal electroactive area for several simulations was 2.01×10^{-3} cm^2 which is around of 100 times lower than the geometric area used in the experimental measurements, which is a common relation reported in literature [13].

As it is observed in Fig. 5a, the numerical solution of the model adequately predicts the typical shape of cyclic voltammograms. On the other hand, the prediction of I_p adequately reproduces the linear behavior with non-zero intercept observed in the experimental measurement as it is shown in Fig. 5b. Furthermore, a statistical analysis based on Fisher's least significance differences for the experimental and theoretical behavior of cathodic and anodic peak responses reveals that both are similar within 95% confidence interval. Thus, the model proposed in (12) and its treatment to obtain the current response given by Eq. (13) adequately describe the electrochemical response of solid M′HCF and support the idea that the non-zero intercept observed in Fig. 5b cannot be ignored in order to apply simplified models such as the Randles-Ševčík.

Even though the model successfully describes the peak current obtained from the voltammograms, its solution by numerical methods limits its practical application. Thus, an analytical solution that explicitly relates the current as a function of interfacial parameters such as electroactive area, diffusion coefficient, bulk concentration, or the number of electrons included in the reaction is preferred.

The model could be analytically solved if the condition (12d) is simplified. In order to evaluate this possibility, the contribution of each term included in the Nernst equation (7) is evaluated numerically. Figure 6 shows each of these contributions, where potential and time are related by (9). As it is observed, $E^{\circ\prime}$ and $\frac{RT}{nF}\ln\left(\frac{X_\omega(t)}{1-X_\omega(t)}\right)$ remain practically constant in the entire evaluated polarization range, while $\frac{RT}{nF} ln\,[C_{M^+}(0,t)]$ shows a linear behavior with a positive slope. Considering the constant behavior of both $E^{\circ\prime}$ and $\frac{RT}{nF}\ln\left(\frac{X_\omega(t)}{1-X_\omega(t)}\right)$, it is possible to combine them into a new parameter, defined as *apparent formal potential* $E^{\circ\prime\prime}$

$$E^{\circ\prime\prime} = E^{\circ\prime} + \frac{RT}{nF}\ln\left(\frac{X_\omega(t)}{1-X_\omega(t)}\right) \tag{17}$$

If Eq. (17) is considered instead of Eq. (8), and applying a similar mathematical derivation to the one shown in (9-11), then condition (12d) can be rewritten as

$$C_{M^+}(0,t) = C^*_{M^+}\exp(-bt) \tag{18}$$

Figure 7 shows a graphical concentration profile at $x = 0$ for the comparison between the original condition (12d) and the simplified one in (18), both calculated numerically at 20 mV s^{-1}. The same behavior is noticeable at other studied polarization scan rates. As it is observed, slight differences between both curves are perceived between 2 and 8 s. These differences are associated to the preexponential term $\frac{1-X_\omega(t)}{X_\omega(t)} \times \frac{X_\omega^{eq}}{1-X_\omega^{eq}}$ presented in condition (12d) that favors a slower decrement of $C_{M^+}(0,t)$ in comparison with the one obtained with condition (18).

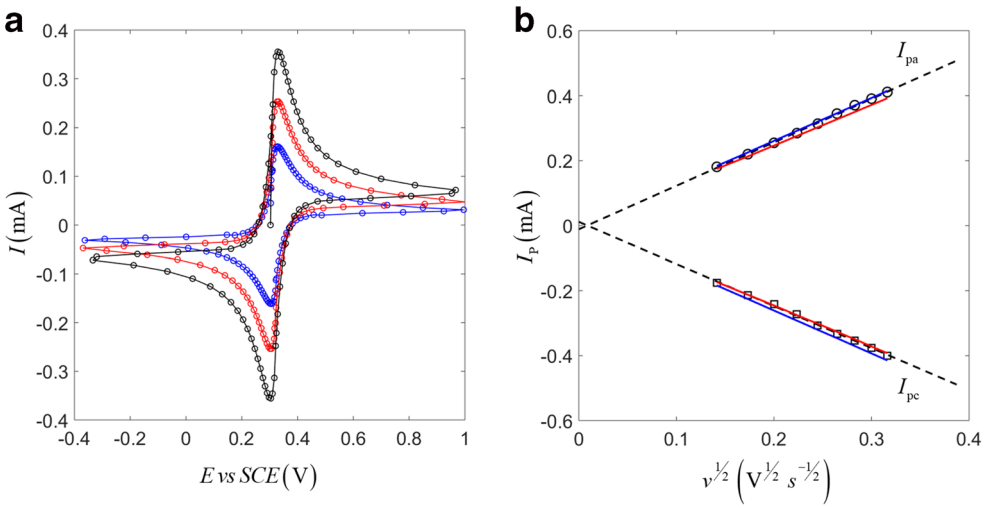

Fig. 5 **a** Theoretical voltammograms obtained by model (12) at v=20, 50, and 100 mV s^{-1} in blue, red, and black lines, respectively. **b** I_{pa}, I_{pc} vs. $v^{1/2}$: experimental data (black), theoretical planar diffusion (blue), solving model (12) considering molar fraction as a function of time (red)

Equation (12a) with the conditions (12b), (12c), and (18) constitutes a simplified model describing the electrochemical response of a M′HCF modified electrode in an electrolyte solution. The simplified model can be solved analytically in planar and spherical coordinates.

Analytical solution for a simplified model: planar coordinates

Using the Laplace transform method and applying the conditions (12b), (12c), and (18), the solution of Eq. (12a) in planar coordinates gives

$$\widetilde{C_{M^+}}(x,s) = \frac{C^*_{M^+}}{s} + \left(\frac{C^*_{M^+}}{s+b} - \frac{C^*_{M^+}}{s}\right)\exp\left(-\sqrt{\frac{s}{D_{M^+}}}x\right) \quad (19)$$

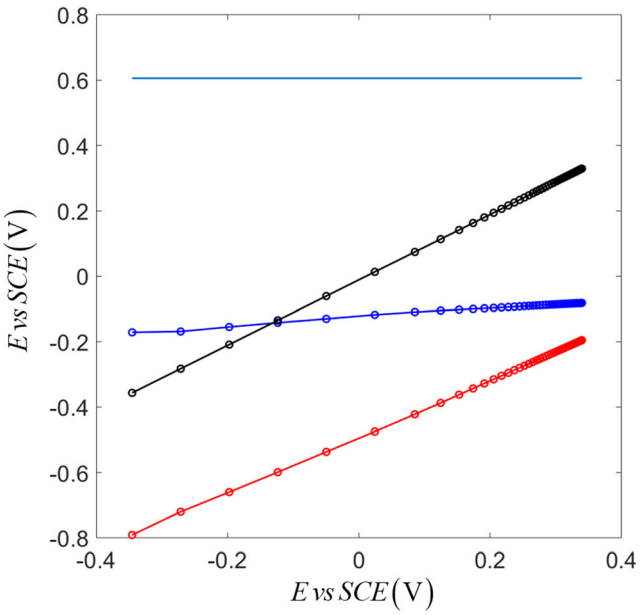

Fig. 6 Potential contribution of each term in Eq. (7), $E^{\circ'}$ (cyan), $\frac{RT}{nF}\ln\left(\frac{X_\omega(t)}{1-X_\omega(t)}\right)$ (blue), $\frac{RT}{nF}\ln[C_{M^+}(0,t)]$ (red), total potential E (black)

Then, transforming Eq. (13) and by inserting it in Eq. (19), it is possible to predict the diffusion current $\widetilde{I(s)}$ at the electrode surface in the Laplace domain:

$$\widetilde{I(s)} = nFAD_{M^+}\left[\frac{\partial\widetilde{C_{M^+}}(x,s)}{\partial x}\right]_{x=0} = nFAC^*_{M^+}\sqrt{\frac{D_{M^+}}{s}} - nFAC^*_{M^+}\sqrt{D_{M^+}}\frac{\sqrt{s}}{s+b} \quad (20)$$

Equation (20) was inversely transformed using WolframAlpha® allowing to obtain the current expression in the time domain:

$$I(t) = nFAC^*_{M^+}(D_{M^+}b)^{1/2}\sigma(bt) \quad (21a)$$

$$\sigma(bt) = \exp(-bt)erfi\left(\sqrt{bt}\right) \quad (21b)$$

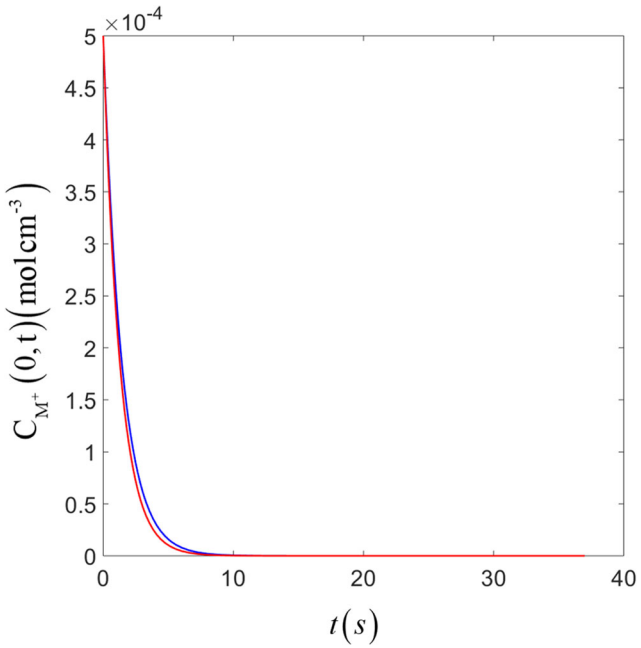

Fig. 7 Comparison between concentration profiles provided by (12d) (blue) and considering ideal planar diffusion (18) (red)

where erfi is the imaginary error function defined as

$$erfi(z) = \frac{2}{\sqrt{\pi}}\int_0^z \exp\left(y^2\right)\mathrm{d}y = -j\cdot \mathrm{erf}(jz) \tag{22}$$

where j is the imaginary unit, $\sqrt{-1}$.

As it is noticed, the mathematical structure of expression (21a) is similar to the one obtained by Randles [18], Ševčík [19], and Nicholson and Shain [20], then (21b) is strongly related to Dawson's function, Daw(z), [29] defined as follows:

$$\mathrm{Daw}(z) = \exp\left(-z^2\right)\int_0^z \exp\left(y^2\right)\mathrm{d}y = \frac{\sqrt{\pi}}{2}\exp\left(-x^2\right)erfi(z) \tag{23}$$

and it is analogous to the current function proposed in [20]. Figure 8 shows the behavior of the $\sigma(bt)$ function.

As it is observed, $\sigma(bt)$ reaches its maximum value at 0.6105 and bt = 0.8540 which is 1.37 times bigger than the one predicted by the current function in the Randles-Ševčík model corresponding to 0.4463 [20], so the differences by considering reaction (1) instead of reaction (3) are considerable.

If Eq. (21b) is solved for its maximum, it is possible to obtain an expression for I_p:

$$I_p = 0.6105nFAC^*_{M^+}\left(D_{M^+}\frac{nF}{RT}v\right)^{1/2} \tag{24}$$

Despite its similarity, Eq. (24) should not be confused with the Randles-Ševčík equation. Equation (24) is more appropriate than the Randles-Ševčík equation when reaction (3) is considered instead of reaction (1).

On the other hand, the E_p corresponding to (24) can be obtained by expressing the Nernst equation at the equilibriums as

$$E_{eq} = E^{\circ\prime} + \frac{RT}{nF}\ln\left(C^*_{M^+}\right) \tag{25}$$

Then, substituting (25) in (9) gives

$$E = E^{\circ\prime} + \frac{RT}{nF}\ln\left(C^*_{M^+}\right) - vt \tag{26}$$

Finally, the evaluation of (26) at the vt value where $\sigma(bt)$ reaches its maximum corresponds to

$$vt = 0.8540\frac{RT}{nF} \tag{27}$$

Generating an expression for E_p gives

$$E_p = E^{\circ\prime} + \frac{RT}{nF}\ln\left(C^*_{M^+}\right) - 0.8540\frac{RT}{nF} \tag{28}$$

Equations (24) and (28) are useful because they show the explicit relationship between electrical properties, I_p and E_p, and experimental variables such as $C^*_{M^+}$, n, A, D_{M^+}, and T. For instance, Eq. (24) shows the linear behavior of I_p as a function of $v^{1/2}$, with a slope equals to $0.6105nFAC^*_{M^+}\left(D_{M^+}\frac{nF}{RT}\right)^{1/2}$. This behavior is useful in practical or analytical applications to determine either n, A, or D_{M^+}. However, it should be noticed that Eq. (24) predicts an intercept equal to zero, which does not correspond to the experimental data (Fig. 5b). This deviation is caused by the changes of mole fraction of the oxidized and reduced species given by the term $\frac{1-X_\omega(t)}{X_\omega(t)}\frac{X^{eq}_\omega}{1-X^{eq}_\omega}$, which was assumed equals to one in the simplified model, as it can be seen in condition (18).

In this manner, I_p as a function of $v^{1/2}$ will reach higher values than those obtained in experimental measurements; however, the same slope will be attained in both cases, as observed in Fig. 5b.

Analytical solution for the simplified model: spherical coordinates

Fick's second law given in (12a) in spherical coordinates is written as follows:

$$\frac{\partial C_{M^+}(r,t)}{\partial t} = D_{M^+}\left[\frac{\partial^2 C_{M^+}(r,t)}{\partial r^2} + \frac{2}{r}\frac{\partial C_{M^+}(r,t)}{\partial r}\right] \tag{29}$$

Solving Eq. (29) is useful to understand the alkali cation concentration and insertion into the M′HCF lattice on spherical modified electrodes of r_0 radius.

By performing a variable substitution, Eq. (29) becomes in planar coordinates:

$$C_{M^+}(r,t) = \frac{w(r,t)}{r} \tag{30}$$

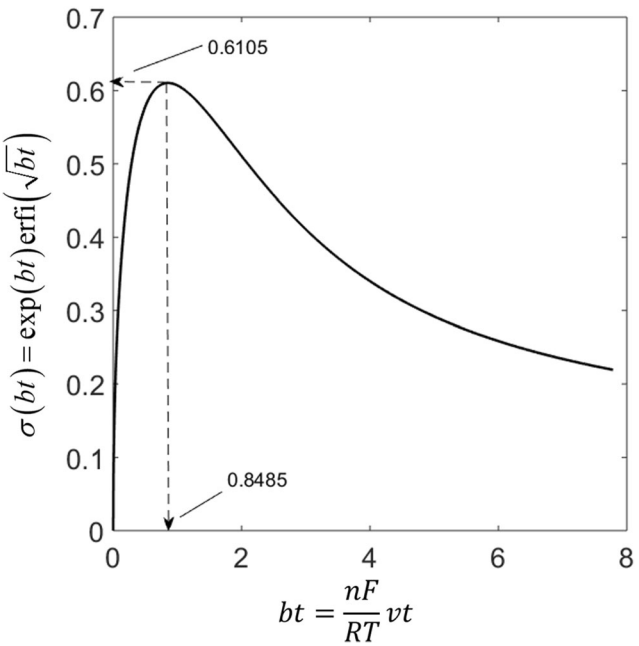

Fig. 8 Current function for an ideal planar electrode according to Eq. (21b)

where $w(r, t)$ is an auxiliary function to be determined. Substituting (30) in (29) and using the conditions (12b), (12d), and (18) lead to the next boundary problem, which has to be solved:

$$\frac{\partial w(r,t)}{\partial t} = D_{M^+}\frac{\partial^2 w(r,t)}{\partial r^2} \tag{31a}$$

$$w(r,0) = rC^*_{M^+} \tag{31b}$$

$$\lim_{r\to\infty} w(r,t) = rC^*_{M^+} \tag{31c}$$

$$w(r_0,t) = rC^*_{M^+}\exp(-bt) \tag{31d}$$

By applying a similar strategy to the one presented for the planar coordinates and inverting the change of variable described in (30), the following current-time expression in spherical coordinates is obtained:

$$I(t) = nFAC^*_{M^+}(D_{M^+}b)^{1/2}\sigma(bt) + \frac{nFAD_{M^+}C^*_{M^+}}{r_0} \tag{32}$$

Equation (32) includes two terms: the first one corresponds to the solution of the problem for a planar electrode, Eq. (21a), while the second one is known as the spherical correction and it is similar to that obtained by Nicholson and Shain [20] and Frankenthal [30] for reaction (1) occurring on spherical electrodes.

When Eq. (32) is solved for $\sigma(bt)$ reaching its maximum value, 0.6105, the peak current is predicted as follows:

$$I_p = 0.6105nFAC^*_{M^+}\left(D_{M^+}\frac{nF}{RT}v\right)^{1/2} + \frac{nFAD_{M^+}C^*_{M^+}}{r_0} \tag{33}$$

On the other hand, the E_p is expressed by Eq. (28).

Unlike (24), Eq. (33) possesses a linear behavior with a slope m and intercept i_0 defined as

$$m = 0.6105nFAC^*_{M^+}\left(D_{M^+}\frac{nF}{RT}\right)^{1/2} \tag{34}$$

$$i_0 = \frac{nFAD_{M^+}C^*_{M^+}}{r_0} \tag{35}$$

Thus, the simplified model in spherical coordinates predicts higher I_p values than those predicted in planar coordinates and a non-zero intercept. Furthermore, from a graphical analysis of experimental I_p values measured at several v values, it is possible to obtain the slope m and intercept i_0 by using least square method. Then, from the simultaneous solving of (34) and (35), the diffusion coefficient of the alkali ions and electroactive area can be calculated as follows:

$$D_{M^+} = \left(\frac{0.6105}{4\pi nFC^*_{M^+}m}i_0^2\sqrt{\frac{nF}{RT}}\right)^{2/3} \tag{36}$$

$$A = \frac{4\pi}{\left(\frac{(0.6105)^2 4\pi nFC^*_{M^+}}{m^2}\left(\frac{nF}{RT}\right)i_0\right)^{2/3}} \tag{37}$$

Some comments concerning the simplified model and the experimental response for NiHCF

According to Fig. 5b, the behavior of experimental data of I_p vs. $v^{1/2}$ is linear with non-zero intercept, in good agreement to previous researches [13–16]. This behavior is nearly described by Eq. (24) for a planar electrode, as the one depicted in Fig. 9a, matching adequately in the slope, but differing in the intercept. From an inspection of Eq. (33), it is evident that a non-zero intercept is obtained when spherical diffusion is considered. Diffusion in a spherical geometry is shown in Fig. 9b. Thus, the deviation observed between the experimental data and Eq. (24) is related, in an empirical manner, to two different phenomena: the own nature of the NiHCF modified electrode and the variation of its electroactive area with time. Regarding the nature of the electrode, the distribution of the NiHCF crystals on the carbon paste surface is not perfect, but random, which modifies the geometry of the interface and the diffusion profile as it is depicted, as a first empirical hypothesis, in Fig. 9c. On the other hand, the variation of the electroactive area is a function of time, which is induced by the variation of the mole fraction required in the term $\frac{1-X_\omega(t)}{X_\omega(t)}$ presented in (6), which was considered as constant in (17) to simplify the original model (12) and solved analytically. In this manner, the geometry of the interface formed by the M′HCF crystal and the electrolyte is a preponderant factor in the current response, as was pointed out in [24].

Under the assumption that the interface is represented by Fig. 9c, Eq. (33) was fitted to the experimental data for NiHCF/KNO_3 interface and, with the m and i_0 values obtained, Eqs. (34) and (35) were simultaneously solved to obtain a mean electroactive area of 7.01×10^{-3} cm^2 and a mean diffusion coefficient of 1.05×10^{-6} cm^2/s. The diffusion coefficient of the alkali ion estimated using the spherical coordinate differs by one order of magnitude from that reported in the literature as 1.29×10^{-5} cm^2 s^{-1} [28] and the electroactive area is 3.5 times greater than the one obtained by means of the simulations shown in Section 4.2 with a value of 2.01×10^{-3} cm^2. Thus, the parameters estimated by Eqs. (36) and (37) should be used with suspicion when the geometry is not strictly spherical; however, they can give a first approximation to the real values for systems described by Fig. 9c.

Therefore, the simplified model given in (31) is a coarse approximation and a practical strategy which avoids the numerical solution of model (12) to obtain, on one hand, an analytical expression of I_p as a function of $v^{1/2}$ describing the typical non-zero intercept observed for the charge transfer in

$$KNi[Fe^{(III)}(CN)_6]_{(s)} + K^+_{(aq)} + e^- \rightleftarrows K_2Ni[Fe^{(II)}(CN)_6]_{(s)}$$

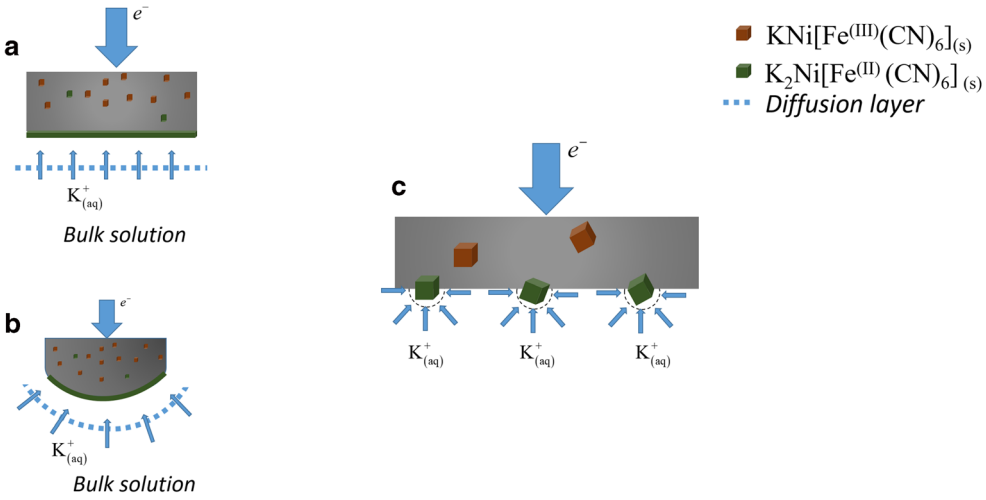

Fig. 9 Schematic representation of a NiHCF modified electrode where the reaction (14) takes place. **a** Planar diffusion of $K^+_{(aq)}$ from bulk to electrode surface. **b** Spherical diffusion of $K^+_{(aq)}$. **c** Hypothetical diffusion of $K^+_{(aq)}$

solid M′HCF and on the other hand, allows, in a simple way, the calculus of attractive useful parameters namely electroactive area and diffusion coefficient of alkali ions.

Conclusions

A thorough revision concerning the Randles-Ševčík theory to understand the electrochemical processes of M′HCF modified electrodes is presented. According to the revision, a rigorous model in planar coordinates to predict the peak currents was proposed, numerically solved, and compared with experimental measurements for NiHCF/ KNO_3 interface. A comparison between the experimental and theoretical I_p as a function of $v^{1/2}$ shows a correlation of 95%, allowing the calculus of the electroactive area of the electrode or the diffusion coefficient of alkali ions in solution using Eq. (24).

Based on experimental evidence, the non-appreciable changes in the term $\frac{1-X_\omega(t)}{X_\omega(t)}\frac{X^{eq}_\omega}{1-X^{eq}_\omega}$ allowed simplifying the proposed model to obtain one, which was solved analytically in planar and spherical coordinates by the Laplace transform method. For both coordinates, the analytical expression for I_p as function of $v^{1/2}$ predicted a linear behavior; however, in the planar coordinates, an intercept equal to zero was obtained, differing to the experimental measurements, while in spherical coordinates, a given intercept was determined. Then, the intercept observed in experimental measurements was associated to the changes in the electroactive area as a function of time, generated by the variations of the mole fraction of the M′HCF, which in turn could favor a radial-like diffusion rather than a planar one.

It is shown that, even with the simplifications, the analytical solution is useful to calculate, in a simple way and as a first approximation, parameters such as the electrode electroactive area and diffusion coefficient of a particular ion inserting into the M′HCF lattice, since it predicts the behavior of the slope that is obtained experimentally when I_p as a function of $v^{1/2}$ is plotted.

Although this paper presents the theory for the example of solid hexacyanoferrates, it is highly probable that the theory is equally applicable for all other insertion electrochemical systems, where the solid electroactive material is dispersed on an electrode surface

Glossary

Symbol	Meaning	Units
A	Area	cm^2
a_i	Activity of specie i	None
b	$\frac{nF}{RT}v$	s^{-1}
C_i	Concentration of species i	mol cm^{-3}
C^*_i	Bulk concentration of species i	mol cm^{-3}
$\widetilde{C}_i(x,s)$	Laplace-transformed concentration	mol s cm^{-3}
D_i	Diffusion coefficient of species i	cm^2 s^{-1}
e^-	Electron	None
E	Potential of an electrode versus a reference	V
$E°$	Standard potential of an electrode	V
$E°'$	Formal potential of an electrode	V
$E°''$	Apparent formal potential of an electrode	V
E_{eq}	Equilibrium potential of an electrode	V
E_p	Peak potential	V
F	Faraday's constant	C mol^{-1}
γ_i	Activity coefficient for species i	none
i_0	Straight line intercept in (33) $\frac{nFAD_{M^+}C^*_{M^+}}{r_0}$	A
I	Current	A
I_p	Peak current	A

I_{pa}	Anodic peak current	A
I_{pc}	Cathodic peak current	A
$\widetilde{I(s)}$	Laplace-transformed current	A s
m	Straight line slope in (33)	A $s^{1/2}$ $V^{-1/2}$
n	Stoichiometric number of electrons involved in the electrode reaction	None
$(Q_a)_v$	Total anodic charge, experimentally obtained, for a scan rate v	C
$Q_a(t)\|_v$	Total anodic charge, experimentally obtained, for a scan rate v as a time function	
$(Q_c)_v$	Total cathodic charge, experimentally obtained, for a scan rate v	C
$Q_c(t)\|_v$	Cathodic charge, experimentally obtained, for a scan rate v as a time function	
r	Radial distance from the center of the electrode	cm
r_0	Radius of an spherical electrode	cm
R	Gas constant	J mol^{-1} K^{-1}
s	Laplace's variable	s^{-1}
t	Time	s
T	Absolute temperature	K
v	Linear potential scan rate	V s^{-1}
$w(r, t)$	Auxiliary function	mol cm^{-2}
x	Coordinate away from the electrode	cm
X_i	Molar fraction of species i	None
$X_i(t)$	Molar fraction of species i as a time function	None
X_i^{eq}	Molar fraction of species i at equilibrium	None

Acknowledgments O. A. González-Meza is grateful to CONACyT for the financial support for his Ph. D. Studies (CVU: 665472).

The authors wish to dedicate this work and its results to Prof. Dr. Fritz Scholz as a deep and sincere acknowledgment to his valuable contribution to the field of the electrochemistry of metal hexacyanoferrates.

References

1. Miller JS (2000) Inorg Chem 39:4392–4408
2. Ohkoshi Shin-ichi. Abe Y, Fujishima A, Hashimoto K (1999) Phys Rev Lett 82:1285–1288
3. Entley WR, Girolami GS (1994) Inorg Chem 33:5165–5166
4. Carpenter MK, Conell RS (1990) J Electrochem Soc 137:2464–2467
5. Duek EAR, De Paoli MA, Mastragostino M (1992) Adv Mater 4: 287–291
6. Itaya K, Uchida I, Toshima S (1983) J Phys Chem 87:105–112
7. Kaneko M, Okada T (2008) Molecular catalyst for energy conversion. Springer
8. Itaya K, Akahoshi H y, Toshima S (1982) J Am Chem Soc 104: 4767–4772
9. Zhao F, Zhang J, Hou X, Abe T, Kaneko M (1998) J Chem Soc Faraday Trans 94:277–281
10. Neff VD (1985) J Electrochem Soc 132:1382–1384
11. Paolella A, Faure C, Timoshevskii V, Marras S, Bertoni G, Guerfi A, Vijh A, Armand M, Zaghib K (2017) J Mater Chem 5:18919–18932
12. Retter U, Widmann A, Siegler K, Kahlert H (2003) J Electroanal Chem 546:87–96
13. Kahlert H, Retter U, Lohse H, Siegler K, Scholz F (1998) J Phys Chem B 102:8757–8765
14. Heli H, Majdi S, Sattarahmady N (2010) Sens Actuators B Chem 145:185–193
15. Siang-Fu H, Lin-Chi C (2012) Sol Energy Mater Sol Cells 104:64–74
16. Gholivand MB, Azadbakht A (2011) Electrochim Acta 56:10044–10054
17. Bard AJ, Faulkner LR (2002) Electrochemical methods fundamental and applications. Willey and sons, John
18. Randles JEB (1948) Trans Faraday Soc 44:327–338
19. Ševčík A (1948) Collect. Czech Chem Commun 13:349–377
20. Nicholson RS, Shain I (1964) Anal Chem 36:706–723
21. Bárcena-Soto M, Scholz F (2002) J Electroanal Chem 521:183–189
22. Orazem ME, Tribollet B (2008) Electrochemical impedance spectroscopy. The electrochemical Society Series, Willey
23. Lovrić M, Scholz F (1997) J Solid State Electrochem 1:108–113
24. Schröder U, Oldham KB, Mylan J, Mahon P, Scholz F (2000) J Solid State Electrochem 4:314–324
25. Lovrić M, Hermes M, Scholz F (1998) J Solid State Electrochem 2: 401–404
26. Scholz F, Dostal A (1996) Angew Chem Int Ed in Engl 34:2685–2687
27. Ellis D, Eckhoff M, Neff VD (1981) J Phys Chem 85:1225–1231
28. Gordon AR (1937) J Phys Chem 5:522–526
29. Dawson HG (1898) Lond Math Soc s1-29:519–522
30. Frankenthal RP, Shain I (1956) J Am Chem Soc 78:2969–2973